

A Search for Metal-poor Stars Pre-enriched by Pair-instability Supernovae

I. A Pilot Study for Target Selection from Sloan Digital Sky Survey (SDSS)

J. Ren^{1,2,3}, N. Christlieb² and G. Zhao^{1,3}

¹ The School of Space Science and Physics, Shandong University at Weihai, Wenhua Xilu 180, 264209 Weihai, Shandong, China;

² Zentrum für Astronomie der Universität Heidelberg, Landessternwarte, Königstuhl 12, D-69117 Heidelberg, Germany; *N.Christlieb@lsw.uni-heidelberg.de*

³ Key Lab of Optical Astronomy, National Astronomical Observatories, Chinese Academy of Sciences A20 Datun Road, Chaoyang, Beijing 100012, China. *renjing@bao.ac.cn; gzhao@nao.cas.cn*

Abstract We report on a pilot study on identifying metal-poor stars pre-enriched by Pair-Instability Supernovae (PISNe). Very massive, first generation (Population III) stars ($140 M_{\odot} \leq M \leq 260 M_{\odot}$) end their lives as PISNe, which have been predicted by theories, but no relics of PISNe have been observed yet. Among the distinct characteristics of the yields of PISN, as predicted by theoretical calculations, are a strong odd-even effect, and a strong overabundance of Ca with respect to iron and the Solar ratio. We use the latter characteristic to identify metal-poor stars in the Galactic halo that have been pre-enriched by PISN, by comparing metallicities derived from strong, co-added Fe lines detected in low-resolution (i.e., $R = \lambda/\Delta\lambda \sim 2000$) spectra of the Sloan Digital Sky Survey (SDSS), with metallicities determined by the SDSS Stellar Parameters Pipeline (SSPP). The latter are based on the strength of the Ca II K line and assumptions on the Ca/Fe abundance ratio. Stars are selected as candidates if their metallicity derived from Fe lines is significantly lower than the SSPP metallicities. In a sample of 12,300 stars for which SDSS spectroscopy is available, we have identified 18 candidate stars. Higher resolution and signal-to-noise ratio spectra of these candidates are being obtained with the Very Large Telescope of the European Southern Observatory and the XSHOOTER spectrograph, to determine their abundance patterns, and to verify our selection method. We plan to apply our method to the data base of several million stellar spectra to be acquired with the LAMOST telescope in the next five years.

Key words: stars: Population II, Population III – stars: supernovae (PISNe) – stars: abundance – stars: chemically peculiar – method: data analysis – techniques: spectroscopic – instrumentation: spectrographs

1 INTRODUCTION

The first generation of stars (hereafter Population III stars) in the Universe formed several hundred million years after the Big Bang. If such stars have survived until today, they can provide us via their abundance

patterns with information on the chemical composition of the early Universe. Because the formation of Pop. III stars occurred in an environment absent of an efficient cooling agent (such as metals and/or dust, which are present at later times), they are believed to have been much more massive with characteristic masses of $\geq 10 M_{\odot}$, up to possibly several hundred solar masses (see, e.g., Bromm et al. 1999, 2009; Abel et al. 2000; Karlsson et al. 2011), and can reflect the yields of the Big Bang (e.g., Abel et al. 2002; Bromm et al. 2002; Nakamura & Umemura 2002). This is also suggested by simulations of the collapse of primordial molecular clouds (Ostriker & Gnedin 1996). However, some studies have suggested that lower mass stars could form within the gas cluster, due to the fragmentation of the turbulent primordial gas in the minihalos (see e.g., Clark et al. 2011a,b) or due to the protostellar feedback (Hosokawa et al. 2011).

Depending on the mass of the progenitor star, different physical mechanisms lead to the explosion of Pop. III stars at the end of their lives (see Bromm et al. 2003). Their UV radiation contributes to the re-ionization of the Universe, and they enrich their surroundings with metals (e.g., Gnedin & Ostriker 1997; Ferrara et al. 2000; Madau et al. 2001; Mori et al. 2002; Yoshida et al. 2004). Very massive first stars ($140 M_{\odot} \leq M \leq 260 M_{\odot}$) will explode as Pair-Instability Supernovae (PISNe), leading to complete disruption of the progenitors (e.g., Fryer et al. 2001; Heger & Woosley 2002; Lingenfelter et al. 2003), enriching the interstellar medium (ISM,) with heavy elements. Due to their short lives ($\leq 3 My$), PISNe are likely the first objects in the Universe that have enriched the interstellar medium (ISM). In the progenitor stars of PISNe, after central helium burning, the temperature and density in the core support pair-instability, and then a partial collapse happens. The collapse proceeds to efficiently compress the stars's core, until fast implosive oxygen and silicon burning take place due to the overpressure, releasing enough energy to revert the collapse, and the star is completely disrupted with no black hole or other remnants left behind (Heger & Woosley 2002; Fryer et al. 2001). The recently observed object SN 2007bi (Gal-Yam et al. 2009) is hypothesized to have been a PISN.

The fraction of metal-poor stars that have formed directly from material that was enriched by the yields of PISNe is predicted to be very small (Karlsson et al. 2008) and this together with an observational bias may explain why no metal-poor star displaying distinct PISNe signatures have been observed so far (e.g., Christlieb et al. 2002; Cayrel et al. 2004; Cohen et al. 2004; Barklem et al. 2005; Frebel et al. 2005). The majority of Pop. II stars with a dominant contribution from PISNe are predicted to have Ca abundances in excess of $[Ca/H] = -2.6$, which implies that a significant fraction of the PISN-dominant stars may have escaped detection (Karlsson et al. 2008). In the past, wide-angle spectroscopic surveys for metal-poor stars have used the Ca K line as a metallicity indicator, relying on the fact that the vast majority of the metal-poor stars follow a well-defined trend of $[Ca/Fe]$ as a function of $[Fe/H]$ (see Beers et al. 1999). Due to the high $[Ca/Fe]$ produced in PISNe, the metallicity of Pop. II stars pre-enriched by them would therefore be overestimated by about a factor of 40 or more, and hence they would not be selected as metal-poor candidates in these surveys.

The lower side of Fig. 4 of Karlsson et al. (2008) shows a simulation of the predicted distribution of stars for which $> 90\%$ of the total atmospheric Ca abundance is synthesized in PISNe in the $[Fe/Ca]$ - $[Ca/H]$ plane, assuming the number of PISNe occupied 10% of the primordial stellar population. The observation data cover the entire metallicity regime of their model, well reproducing the small scatter in observations (see, e.g., Cayrel et al. 2004; Arnone et al. 2005; Barklem et al. 2005). Among the several hundred well-studied stars falling in the high number density regions in the abundance ratio diagram, none shows the abundance signatures of PISNe. Note that still below $[Ca/Fe] \sim -1$, there is a negligible fraction of PISN-enriched stars. These are the stars that we are targeting with our selection method.

Non-rotating stars exploding as PISNe differ from core-collapse SNe in that they exhibit a neutron excess in their interiors. Consequently, one of the characteristic chemical signatures of PISNe is a strong odd-even effect, which means particularly low abundance ratios of odd- Z elements to even- Z elements. Furthermore, the production of both rapid and slow neutron-capture elements are absent due to the lack of excess neutrons in addition to shorter expansion timescales during the explosion. Other nucleosynthetic signatures of PISNe are $[Mg, Si/Na, Al] \gg 0$; $[Si, S/C] \sim 1-1.5$; $[Zn/Fe] \ll 0$ (Heger & Woosley 2002; Umeda & Nomoto 2002; Karlsson et al. 2011). Hence metal-poor stars pre-enriched by PISNe can be identified by these chemical signatures.

In the Sloan Digital Sky Survey (SDSS), candidate metal-poor stars are selected by means of *ugriz* photometry; therefore, the above-mentioned bias against PISNe pre-enriched stars is not present in the sample of stars for which low-resolution (i.e., $R = \lambda/\Delta\lambda \sim 2000$) spectroscopy was obtained.

The seventh data release of SDSS (DR7) contains 460,000 stars; for about half of them, low-resolution spectra have been acquired. According to Karlsson et al. (2008), the number fraction of second-generation stars below $[\text{Ca}/\text{H}] = -2.0$ with a dominant (i.e. $> 90\%$) contribution from PISNe is 10^{-4} to 5×10^{-4} . About 10 % of these PISN-dominated stars are predicted to have $[\text{Fe}/\text{Ca}] \sim -1$. Therefore, according to the current model (Karlsson et al. 2008), at least two stars and up to 9–16 stars with dominant pre-enrichment by PISNe could be found in DR7.

After verifying our method by this pilot study, we will also apply the method to DR8 and future SDSS data releases, as well as to the several million stellar spectra to be obtained in the course of the LAMOST (The Large Sky Area Multi-Object Fiber Spectroscopic Telescope) Galactic survey (Zhao et al. 2012), which will provide more candidates. If we can find any stars pre-enriched by PISNe, this would provide observational evidences for their existence; otherwise an upper limit for their space density can be derived.

In this paper we report on the candidate selection applied to SDSS DR7. In section 2, we give a brief description of the star sample from SDSS DR7; Section 3 introduces the metallicities from SSPP; the data analysis process and candidates selection are described in section 4 and 5, respectively; Finally a conclusion is given in section 6.

2 THE SDSS SAMPLE

The observations forming the basis of SDSS-DR7 were carried out during an eight-year period with a dedicated 2.5-m telescope located at Apache Point Observatory in Southern New Mexico. DR7 includes photometric data of 460,000 stars and over 300,000 stellar spectra covering more than 8200 square degrees of the sky. The wavelength coverage is 3800–9200 Å, with a resolving power of $R = 1800$ –2200 and $S/N > 4$ per pixel at $g = 20.2$. We extracted 224,080 stars from the table *star* joining to *sppParams* in SDSS-DR7 using *CasJobs*, which is the online workbench for extracting large scientific catalogs. The number reduced to 17,623 when narrowing the temperature range to 4500–6500 K, and requiring the average signal-to-noise ratio (S/N) per pixel of more than 20 in the wavelength range 4000–8000 Å. We adopted this temperature range by inspection of the feasibility of our method on different spectra. After the data analysis, about 5,000 spectra were rejected due to lack of flux points in the wavelength range which contains the iron lines we use. The final sample to which we applied our selection criteria hence consists of 12,304 stars.

When this work was under preparation, the SDSS Data Release 8 (DR8) was published. Besides adding more spectra of stars to the data release, the final adopted values of T_{eff} and $\log g$ are only slightly different from DR7, while the $[\text{Fe}/\text{H}]$ estimates are in general improved, especially at the low-metallicity (< -3.0) and high-metallicity (> 0.0) ends, due to a re-calibration of the NGS1 and NGS2 parameter estimation approaches (see Table 1), and changes in S/N and $(g-r)_0$ (Smolinski et al. 2011). Therefore, the primary sample selection based on T_{eff} and $\log g$ is still valid, but we consider the $[\text{Fe}/\text{H}]$ from DR8 instead of DR7. The $[\text{Fe}/\text{H}]$ from DR7 and DR8 are both listed in Table 3.

3 METALLICITIES DERIVED BY THE SSPP

SSPP is the stellar parameter pipeline developed for the Sloan Extension for Galactic Exploration and Understanding (SEGUE), which is a part of SDSS-II and SDSS-III. This pipeline works on low-resolution spectroscopy and *ugriz* photometry obtained during the course of SDSS-I, SDSS-II/SEGUE-1 and SDSS-III/SEGUE-2, making use of multiple techniques to estimate fundamental stellar atmospheres parameters (including effective temperature, surface gravity, and metallicity), along with determining radial velocities for AFGK-type stars (Lee et al. 2008a,b; Allende Prieto et al. 2008; Smolinski et al. 2011). Different approaches were applied for each parameter, as summarized in Table 1. For $[\text{Fe}/\text{H}]$, 12 different methods were adopted in SSPP.

Table 1 Metallicity estimation methods used by the SSPP

| VALUE | METHOD | DESCRIPTION |
|-------|--------|----------------------------------------------------------------------------------------------------------------------------------------------------------------------|
| feh1 | NGS2 | χ^2 minimization technique using Kurucz NGS α -enhanced grid ¹ |
| feh2 | NGS1 | χ^2 minimization technique using Kurucz NGS non- α -enhanced grid ¹ |
| feh3 | ANNSR | Neural network trained on synthetic spectra ¹ |
| feh4 | ANNRR | Neural network trained on real spectra ² |
| feh5 | CaHK1 | Spectral fitting in the range $\lambda = 3850\text{--}4250 \text{ \AA}$, using the NGS1 grid ¹ |
| feh6 | CaHK2 | Ca II K line strength combined with a broadband colour ³ |
| feh7 | CaHK3 | Neural network approach using the Ca K line index K24 and $g - r$ ¹ |
| feh8 | ACF | Autocorrelation function proportional to the frequency and strength of weak metallic lines ³ |
| feh9 | CaIT | Strength of the Ca II triplet lines and $B - V$; neural network approach ⁴ |
| feh10 | WBG | Equivalent width of the Ca II K line and comparison of weaker metallic lines ⁵ |
| feh11 | k24 | matching of synthetic spectra using k24 grid of flux with the observed flux in the region $\lambda = 4400\text{--}5500 \text{ \AA}$, including $g - r$ ⁶ |
| feh12 | ki13 | matching synthetic spectra using ki13 grid of flux without colour with the observed flux in the region $\lambda = 4400\text{--}5500 \text{ \AA}$ ¹ |
| feha | ADOP | Adopted [Fe/H] value, combination of good estimates |

¹ Lee et al. 2008a² Re Fiorentin et al. 2007³ Beers et al. 1999⁴ Cenarro et al. 2001a,b⁵ Wilhelm et al. 1999⁶ Allende Prieto et al. 2006

Each of these methods only works for a certain colour range and S/N level. More detailed information can be found in Table 5 of Lee et al. (2008a). Among these approaches, *feh6* and *feh7* use the strength of Ca II K line in combination with a broadband colour to estimate [Fe/H] (Beers et al. 1999; Lee et al. 2008a). *feh9* was obtained by measuring the integrated strength of Ca II triple features, which are also sensitive to $\log g$, along with the de-reddened $B - V$ colour (Cenarro et al. 2001a,b). *feh5* applied the NGS1 grid to a short wavelength window covering Ca II K, Balmer lines, and a Ca I line, to estimate the metallicity, temperature and surface gravity, respectively (Lee et al. 2008a). *feh10* uses a combination of the equivalent width of Ca II K line and a comparison of weaker metallic lines to synthetic spectra (Wilhelm et al. 1999). The adopted *feha* containing the information of Ca abundance as well as other weak metal lines, is much closer to the theoretical definition of metallicity. A flag value 0 is assigned to the result from each method if the star does not satisfy the range of validity for this method, or 1 if it is defined as an outlier after matching with the synthetic spectra (See Lee et al. 2008a; Smolinski et al. 2011).

In order to make the comparison more sensitive to the deviation between the abundance of calcium and iron, we use the averaged value of *feh6* and *feh7*, if they are both valid, as indicated by a flag value of 2; or the valid one of them. Otherwise, one of *feh9*, *feh10* and *feh5* would be used, depending on the given priority, which is based on the correlation degree to Ca abundance. In the case that none of them passed the synthetic spectra matching check, the adopted *feha* was used.

4 METALLICITY FROM COADDED IRON LINES

The metallicity Z of a star refers to the proportion of its matter made up of chemical elements heavier than helium. Iron is often used as the reference element for metallicity, since it is the end product of exothermic nucleosynthesis in stars, and because numerous iron lines are present in the optical wavelength region, so that its abundance can easily be measured in high-resolution spectra of cool stars. However, if the metallicity is to be determined from low resolution spectra, one has to resort to the much stronger Ca II H and K lines and assumptions on the relation between [Fe/H] and [Ca/H] (See, e.g., Beers et al. 1999).

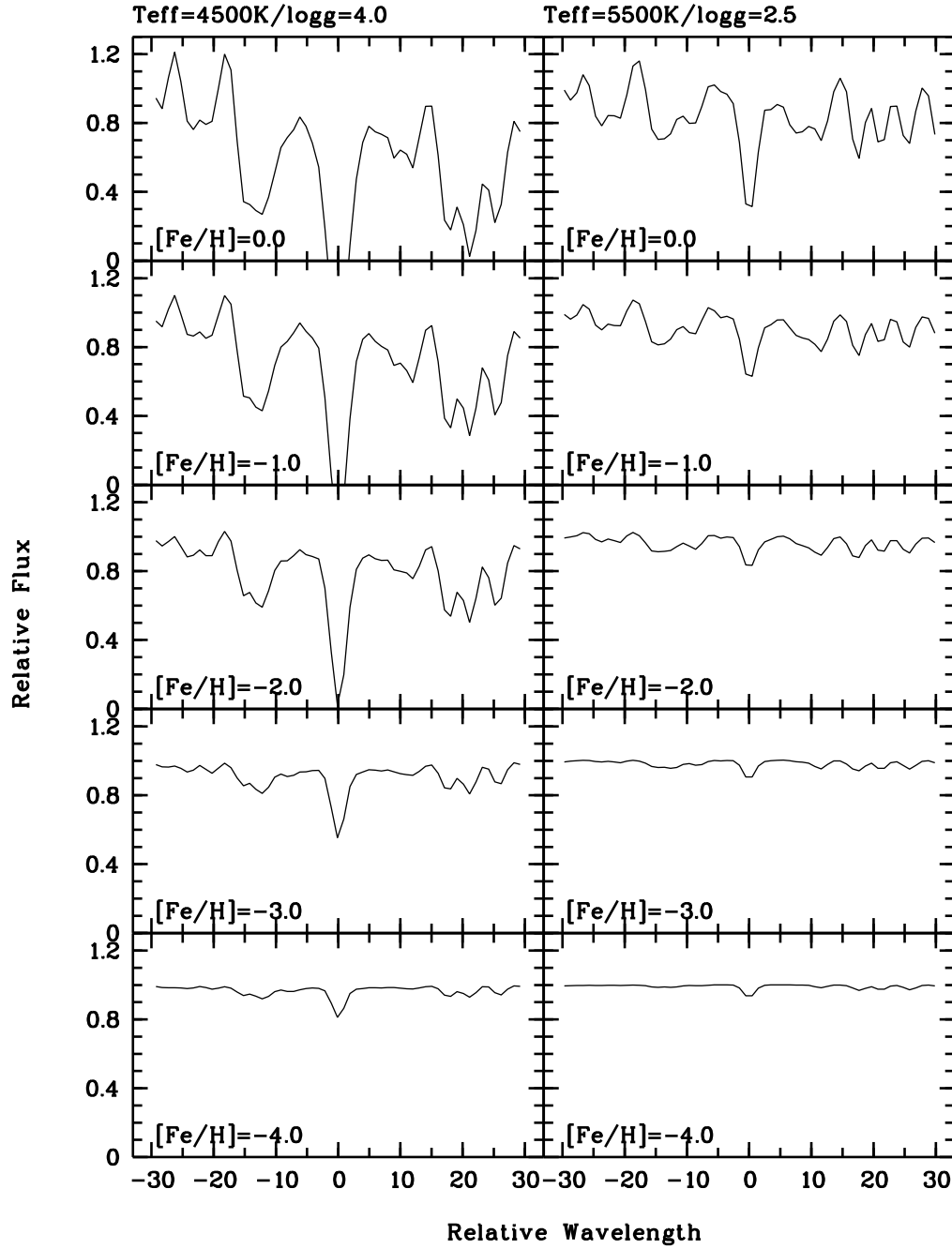


Fig. 1 The result of coadding iron lines in synthetic spectra with different $[\text{Fe}/\text{H}]$ for $T_{\text{eff}} = 4500/\log g = 4.0$ and $T_{\text{eff}} = 5500/\log g = 2.5$, respectively. The line center is shifted to a wavelength of zero in the rest frame.

Table 2 The two Fe I lines we coadded^a

| λ [Å] | Species | W_{\odot} [Å] | $\log gf$ | ξ [eV] |
|---------------|---------|-----------------|-----------|------------|
| 4045.82 | Fe I | 1.17 | 0.280 | 1.485 |
| 4383.56 | Fe I | 1.01 | 0.200 | 1.485 |

^a $\log(gf)$ and lower excitation energy are from Vienna Atomic Line Database (VALD). The equivalent widths (EW) are the line strength in the Sun.
<http://www.astro.univie.ac.at/~vald/>

4.1 Selecting iron lines

We searched for strong iron lines detectable in SDSS spectra, using identifications of lines in the Solar spectrum (Moore et al. 1966). Because of the limited quality of the SDSS spectra in terms of resolving power and S/N , most of the Fe lines that are very strong in the Sun are difficult to detect in the SDSS spectra. After attempts to identify these lines in spectra of stars with different T_{eff} , $\log g$ and $[\text{Fe}/\text{H}]$, the lines with equivalent widths below 1 Å were rejected. Additionally, because some SDSS spectra have no flux data around 3820 Å, and also because lines at the extreme blue end with wavelength smaller than 4000 Å are usually blended with other lines or completely hidden in the noise, finally, two relatively strong iron lines are left: Fe I 4045.82 Å, and Fe I 4383.56 Å. Their atomic data are listed in Table 2.

Fig. 1 displays the coadded iron lines in synthetic spectra of stars with different metallicities, which demonstrates that they are strong enough to be detected at $[\text{Fe}/\text{H}] \geq -4.0$ and $T_{\text{eff}} \leq 6500\text{K}$. We hence restricted the application of our method to stars in this T_{eff} range. Note that additional information on the metallicity is contained in the continuum around the coadded Fe I lines. Our method implicitly makes use of this information via the continuum bands that are used to scale the synthetic spectra to the observed ones.

4.2 Normalization

Continuum normalization of a spectrum is always a delicate task, even more so when the spectra to be normalized only have a low resolution, and when the task must be performed automatically for stars with a variable range of effective temperatures, which is the case in our application. Because the two iron lines we use both lie in the wavelength range of 4000–4500 Å, only a short wavelength range in the spectrum covering the two iron lines is used. This makes the normalization easier, since a smaller wavelength region has to be modeled. We normalize the spectrum in the region $\lambda = 3820\text{--}5800\text{Å}$, which is a bit larger than the range we use for following analysis, because we want to include more continuum points in the spectrum for a more accurate continuum determination. We adopt the same division of the spectrum as that used for two separate continuum fits in SSPP (Lee et al. 2008), because we want to be consistent with the SSPP analysis process as much as possible, which will make the comparison of the results more robust.

In order to determine an appropriate continuum fit, some strong lines are removed from the spectrum, i.e., Balmer lines, Ca II K lines, Ca I line, Mg Ib lines, G-band and iron lines, after which the spectrum is iteratively fitted to a ninth-order polynomial. We then rejected the points outside the 3σ range of the fitted function after the first fit, which can also remove the cosmic rays. In the following iterations, considering the numerous weak lines left in the spectrum, only points within $2\sigma \sim -0.5\sigma$ range of the fitted function were kept. The final continuum was obtained after four iterations. Fig. 2 shows two examples of the normalization for two observed SDSS spectra, among our candidates.

The synthetic spectra we use were kindly provided by Y. S. Lee (priv. comm.). The wavelength coverage is 3000–10,000 Å in 0.01 Å steps, and they were generated using Kurucz models and the spectrum synthesis program TURBOSPECTRUM. The spectra cover a wide range of the stellar parameters T_{eff} , $\log g$ and $[\text{Fe}/\text{H}]$, from 4000 K to 9750 K, 0.0 to 5.0 dex and -4.0 to 0.5 dex, in steps of 250 K, 0.5 dex,

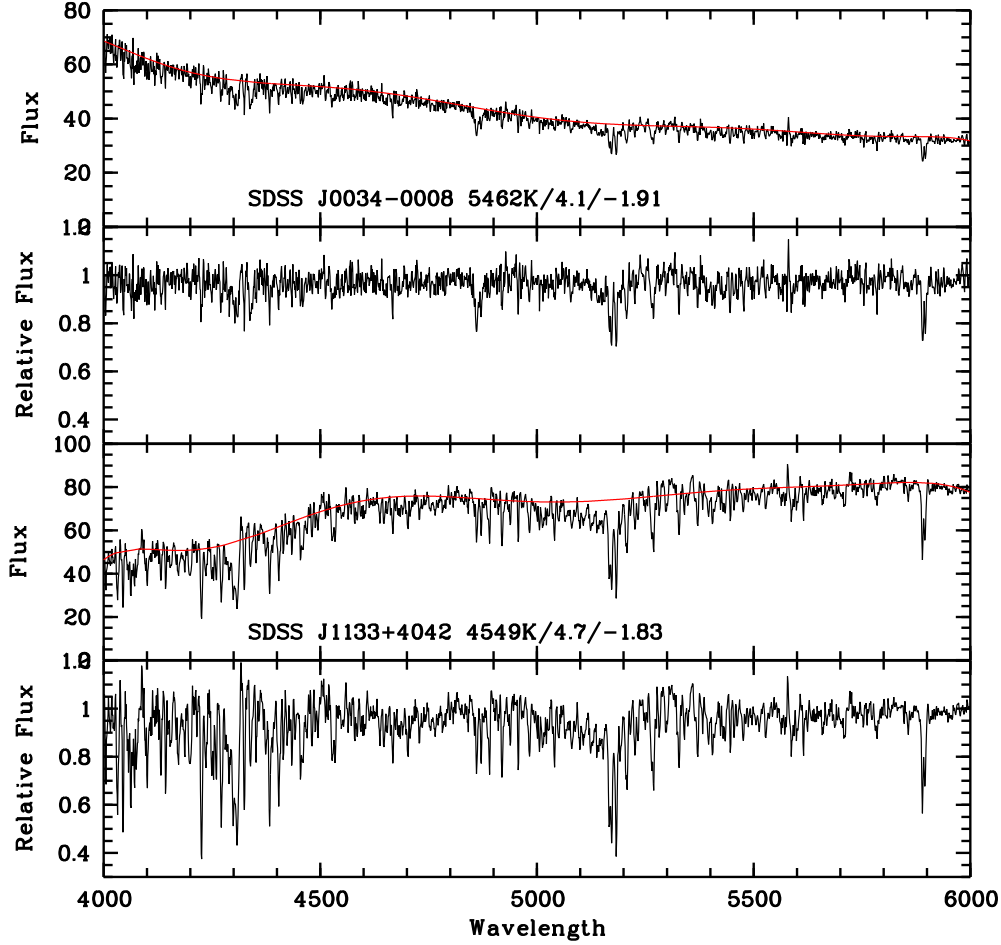


Fig. 2 Continuum determination for SDSS spectra of our two candidates: SDSS J0034–0008 and SDSS J1133+4042.

and 0.5 dex, respectively. The synthetic spectra are processed in exactly the same way as the SDSS spectra, in order to reduce systematic errors.

4.3 Coadding iron lines

Because the wavelength scale used in SDSS spectra is based on vacuum, the first step before coadding the iron lines is to transform the wavelength scale of the original SDSS spectrum to an air-based wavelength scale, and after shifting the spectrum to a zero-velocity rest frame using the radial velocity estimated from matching ELODIE template spectra (Prugniel & Soubiran 2001; Moulata et al. 2004; Adelman-McCarthy et al. 2008), the two iron lines are shifted to a wavelength of zero. The radial velocity from ELODIE is reported to be the best available estimate by previous experiences (Lee et al.

2008a). Linear interpolation is used to put the spectral regions of the two lines on the same pixel scale, before the spectra are coadded. To speed up the analysis process, only ranges of 60 \AA centered on the two iron lines were used. Fig. 3 shows the iron lines detected in the spectra and the strength of the lines after coadding, for both observed and synthetic spectra. The synthetic spectra corresponding to the best-fit metallicity from our analysis and from SSPP are also plotted for comparison. It is clearly seen that the adopted SSPP metallicity is too high for iron lines. It is likely that the SSPP result is dominated by other chemical features other than iron, e.g., Ca II, Mg II, or even the molecular carbon bands for some cases, which we will discuss more later.

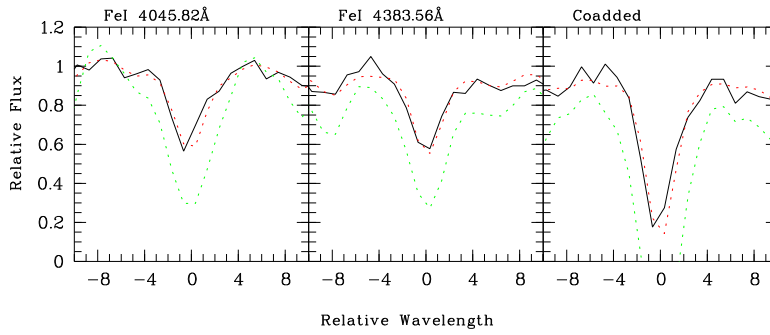


Fig. 3 Line strength before and after coadding two iron lines of an observed spectrum for one of our candidates (solid, SDSS J2118–0613) and the synthetic spectra (dashed, $T_{\text{eff}} = 4750 \text{ K}$, $\log g = 4.5$, $[\text{Fe}/\text{H}] = -2.0/0.0 \text{ dex}$). The red and green dashed line correspond to the best fit synthetic spectrum from our analysis ($[\text{Fe}/\text{H}] = -2.04$) and from SSPP ($[\text{Fe}/\text{H}] = -0.10$), respectively.

4.4 Metallicity determination

Based on the T_{eff} and $\log g$ from SSPP, the corresponding synthetic spectrum was chosen, and then it was degraded and interpolated to the same resolving power ($R \sim 2000$) and wavelength scale as SDSS spectrum. Since the resolution does not change much in the wavelength range we use in this work, we adopted a constant wavelength step width. Then we used a reduced χ^2 criterion to get the best-fit metallicity by minimizing the difference between the observed and synthetic coadded flux. We used a range of 10 \AA of the coadded spectrum, which only covers the coadding feature, centered on the line, in order to reduce the impact from other lines and noise in the rest part of the spectra. A third-order polynomial is adopted to fit all the χ^2 values from different metallicities, and the metallicity corresponding to the minimum χ^2 is taken as the best-fit value.

4.5 Error estimation

In order to estimate the uncertainty of our method, we analyzed 1069 stars belonging to different globular clusters (GCs) and open clusters (OCs). The spectroscopic data were obtained during SEGUE observations and they were used to check the validation of the SEGUE target selection and SSPP (Lee et al.

2008b; Smolinski et al. 2011). Only GC members with $4500 \text{ K} \leq T_{\text{eff}} \leq 6500 \text{ K}$ and $S/N > 20$ were selected in consistency with our sample, as described in Section 2. Finally, 724 stars were considered for eight GCs (M3, NGC 5053, M53, M71, M92, M15, M2, and M13) and five OCs (NGC 6791, M35, M67, NGC 2420, and NGC 2158). The high-resolution metallicity results are from the work of Harris (1996); Dias et al. (2002) and Boesgaard et al. (2009). By comparing the metallicities from our work with the averaged $[\text{Fe}/\text{H}]$ from high-resolution analysis for each cluster, we estimated the uncertainty of our method to be ~ 0.40 dex.

5 CANDIDATES SELECTION

Due to the differences in the methods used, together with the weakness of the Fe I lines, the limited quality of the SDSS spectra, and uncertainties incurred by the automated analysis, our $[\text{Fe}/\text{H}]_{\chi^2}$ estimated directly from Fe I lines expectedly deviates from the SSPP metallicities $[\text{Fe}/\text{H}]_{\text{SSPP}}$. The average deviation is 0.29 ± 0.25 dex. As shown in Fig. 4, at the high and low metallicity ends, larger scatters appear in the comparison. A linear fit $[\text{Fe}/\text{H}]_{\text{SSPP}} = 0.76 \times [\text{Fe}/\text{H}]_{\text{thiswork}} - 0.23$ is performed, with a standard deviation of 0.35 dex, which demonstrates that our result is systematically higher at $[\text{Fe}/\text{H}] > -1.0$. The 3σ outliers based on the linear fit are interesting, despite possible origination from errors. In this work, we care about those objects falling outside 3σ with likely Ca-enhancement, which might be potential candidates for PISNe enriched metal-poor stars. By means of visual inspection of the original and coadded spectra, we rejected false positives from the candidate sample, i.e., spectra suffering from overestimated signal-to-noise ratios or poor continuum determination. Finally, 18 stars were selected as Ca-enhanced candidates. They are listed in Table 3, and shown as red stars in Fig. 4.

The spectra of outliers with lower SSPP metallicity were also inspected, and we found that the large departure is mainly due to low S/N and hence poor continuum determination.

In addition, the outliers are mostly cooler ($T_{\text{eff}} < 5000 \text{ K}$) and metal-poor stars ($[\text{Fe}/\text{H}] \leq -1.00$), therefore, according to Lee et al. (2008a) the estimated metallicity from Ca lines in this case might be underestimated by ~ 0.5 dex, indicating the true departure from our derived results would be even larger.

Although We note that a large fraction of the used $[\text{Fe}/\text{H}]$ values from the SSPP are the final adopted value *feha*, which contains the information of Ca and other metallic lines, e.g., Mg I, Fe I, Na I, the true difference (excluding uncertainty) between the two metallicities can still reflect the deviation of abundance between Fe lines and other metal lines, especially Ca lines, since some weak Ca lines might be used and the final valid metallicity estimators were selected after matching with the synthetic spectrum in the wavelength range of 3850–4250 Å and 4500–5500 Å (Smolinski et al. 2011).

We inspected Ca I 4226 Å, Ca II H and K lines in the spectra of our candidates, and no apparent enhancement of Ca abundance was found on Ca I 4226 Å line, while for Ca II H and K lines, the situation is complicated due to the saturation and blendings. Furtherly, we are not clear about the sensitivity of Ca abundance on the calcium line strength, and whether these stars are influenced by chromospheric activities, thus better quality data are needed to measure the accurate abundances and look into these questions. In Fig. 5, our metallicity results also indicate that there are larger differences between the $[\text{Fe}/\text{H}]$ values of DR7 and DR8 at the low metallicity tail compared to the differences at higher metallicity. The number of stars with a large offset in the comparison between DR8 and our derived $[\text{Fe}/\text{H}]$ increases when a smaller number of estimators is used, and fewer estimators (≤ 3) are used at lower metallicity ($[\text{Fe}/\text{H}] < -3.0$).

In general, our method to derive $[\text{Fe}/\text{H}]$ is reliable, as seen from their good correlation with the metallicity of different approaches used in SDSS-DR8. We also note that only a few selected outliers have valid result from methods using Ca II lines, which weaken the correlation with Ca-enhancement. We do not exclude the possibility that the large departure of our $[\text{Fe}/\text{H}]$ from those derived with the SSPP is caused by errors in either or both of the two estimates. Therefore, it is necessary to acquire spectra of higher resolution and S/N to verify our selection method, and for possibly identifying via their abundance patterns stars pre-enriched by PISNe. To this end, medium-resolution ($R \sim 6000$ –

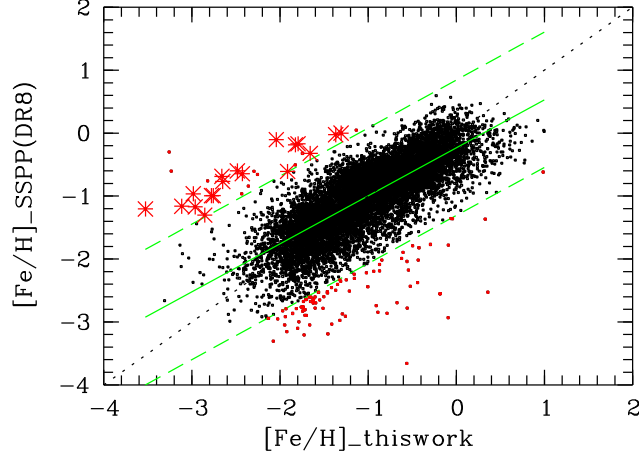


Fig. 4 Comparison between metallicities from SSPP and our method. Those 3σ outliers with $S/N > 25$ (red stars) on the upper side show a possible Ca enhancement. Both the upper and lower 3σ outliers are highlighted in red dots.

11, 000) of our candidates are currently being obtained with the XSHOOTER spectrograph attached to the Unit Telescope 2 of the Very Large Telescope of the European Southern Observatory.

6 CONCLUSIONS

Very massive ($140 M_{\odot} \leq M \leq 260 M_{\odot}$), first generation stars end their lives as PISNe, which have been predicted by theories, but no strong observational evidence for their existence in the early Universe has yet been obtained. The theoretically predicted chemical fingerprints of PISNe are high overabundances of Ca with respect to Fe and the ratio of these elements in the Sun, and a strong odd-even effect. We carried out a pilot study on identifying metal-poor stars with strong Ca-enhancement, by comparing the metallicities determined with the SDSS SSPP containing information on the Ca abundance (i.e., those estimators which involve the Ca II H and K lines or the Ca II infrared triplet) with metallicities we derived directly from iron lines. We used a coadding technique to increase the S/N of the SDSS spectra. A χ^2 minimization method was applied to search the best matched metallicity from a series of synthetic spectra with known atmosphere parameters. Our derived metallicities correlate well with those of the SSPP, with a linear fit $[\text{Fe}/\text{H}]_{\text{SSPP}} = 0.76 \times [\text{Fe}/\text{H}]_{\text{thiswork}} - 0.23$. By applying a 3σ criterion and visual inspection, 18 candidates were selected. Once the nature of these candidates is determined and our selection method is verified, we will apply our method to the low-resolution stellar spectra obtained with the LAMOST telescope.

Acknowledgements We give thanks to Young Sun Lee for kindly offering us the synthetic spectra; Torgny Karlsson and Haining Li are acknowledged for their helpful comments on the manuscripts; we appreciate the stimulating discussions with Yuqin Chen and her helpful suggestions and comments on the manuscripts. J.R. and N.C. acknowledge financial support by the Global Networks program of

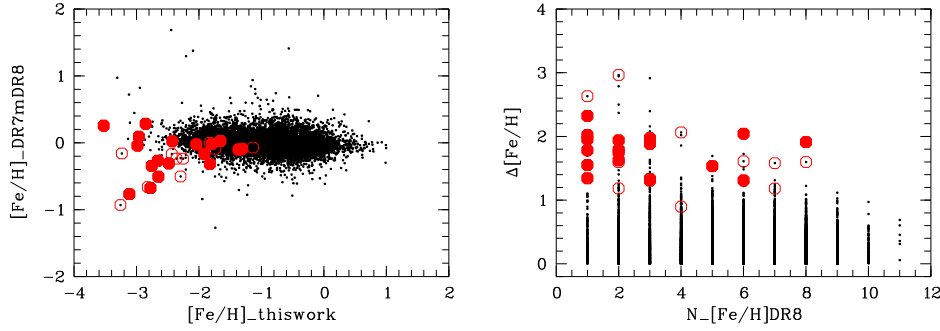


Fig. 5 Left: Metallicity deviation of DR7 from DR8, distributing with our derived metallicity. Right: Metallicity deviation of DR8 from our method, distributing with the number used to give the final metallicity in SSPP DR8. Black dots: the whole sample; red circles: 3σ outliers with higher Ca; red filled circles: selected candidates.

Table 3 Candidates of Metal-poor Stars Pre-enriched by PISNe.

| Star | Plate | MJD | Fiberid | S/N | T_{eff} (K) | $\log g$ | [Fe/H] DR7 | [Fe/H] ^a DR8(Ca) | [Fe/H] this work | Note ^b |
|--------------------------|-------|-------|---------|-----|-------------------------|----------|---------------|--------------------------------|---------------------|-------------------|
| SDSS J081157.13+143533.0 | 2270 | 53714 | 253 | 52 | 4750 | 4.0 | -0.95 | -1.20 | -3.52 | adop, 1 |
| SDSS J015315.91-084216.8 | 0665 | 52168 | 489 | 35 | 4822 | 3.6 | -1.00 | -0.96 | -2.98 | adop, 1 |
| SDSS J211851.04-061319.6 | 0639 | 52146 | 538 | 47 | 4795 | 4.4 | -0.13 | -0.10 | -2.04 | adop, 2 |
| SDSS J030209.90-062704.0 | 0458 | 51929 | 365 | 33 | 4657 | 4.2 | -0.62 | -0.65 | -2.43 | adop, 1 |
| SDSS J121144.01+011951.3 | 0517 | 52024 | 003 | 65 | 4798 | 4.5 | -0.19 | -0.17 | -1.79 | adop, 2 |
| SDSS J205923.08-065208.2 | 0636 | 52176 | 064 | 42 | 5298 | 4.0 | -0.91 | -0.60 | -2.48 | wbg, 3 |
| SDSS J080805.07+183352.0 | 1923 | 53319 | 595 | 31 | 4830 | 4.8 | -1.19 | -0.99 | -2.76 | caik2, 8 |
| SDSS J112238.18+434555.3 | 1365 | 53062 | 144 | 26 | 4808 | 4.5 | -1.11 | -0.77 | -2.65 | caik1, 6 |
| SDSS J164435.94+203659.1 | 1569 | 53168 | 232 | 36 | 4665 | 4.6 | -0.32 | -0.32 | -1.66 | caik1, 6 |
| SDSS J075800.22+435257.9 | 0437 | 51869 | 374 | 60 | 4588 | 4.9 | -0.13 | -0.02 | -1.37 | adop, 1 |
| SDSS J111218.53+262543.8 | 2212 | 53789 | 636 | 43 | 4624 | 5.0 | -0.09 | 0.00 | -1.31 | adop, 3 |
| SDSS J113344.77+404238.4 | 1443 | 53055 | 090 | 36 | 4549 | 4.7 | -0.61 | -0.19 | -1.83 | caik1, 5 |
| SDSS J155219.79-001022.7 | 0342 | 51691 | 038 | 35 | 4662 | 3.9 | -1.70 | -0.99 | -2.78 | caik3, 2 |
| SDSS J104459.32+360554.7 | 2090 | 53463 | 273 | 33 | 5877 | 4.3 | -0.95 | -0.69 | -2.66 | adop, 3 |
| SDSS J095423.10+240410.8 | 2341 | 53738 | 019 | 27 | 5004 | 3.6 | -1.93 | -1.16 | -3.12 | adop, 1 |
| SDSS J230130.60+001920.9 | 0380 | 51792 | 499 | 30 | 4798 | 4.5 | -1.08 | -1.17 | -2.96 | adop, 2 |
| SDSS J153642.56+210747.4 | 2166 | 54232 | 266 | 31 | 5489 | 4.2 | -1.02 | -1.30 | -2.85 | adop, 1 |
| SDSS J003416.18-000849.9 | 0392 | 51793 | 224 | 27 | 5462 | 4.1 | -0.75 | -0.61 | -1.91 | wbg, 3 |

^a : [Fe/H] of DR8(Ca) refers to the Ca-related metallicity from SSPP(DR8) used in this work.

^b : This column list the method used to determine [Fe/H]-DR8(Ca) and the number of valid methods in SSPP.

Universität Heidelberg, and by Deutsche Forschungsgemeinschaft through grant CH 214/5-1 as well as Sonderforschungsbereich SFB 881 “The Milky Way System” (subproject A4). J.R. and G.Z. acknowledge the support by NSFC grant No. 10821061. J.R. acknowledges partial financial support from the Shandong University Fund for Graduate Study Abroad.

References

- Abel, T., Bryan, G. L., & Norman, M. L. 2000, *ApJ*, 540, 39
 Abel, T., Bryan, G. L., & Norman, M. L. 2002, *Science*, 295, 93

- Adelman-McCarthy, J. K., Agüeros, M. A., Allam, S. S., et al. 2008, *ApJS*, 175, 297
- Allende Prieto, C., Beers, T. C., Wilhelm, R., et al. 2006, *ApJ*, 636, 804
- Allende Prieto, C., Sivarani, T., Beers, T. C., et al. 2008, *AJ*, 136, 2070
- Arnone, E., Ryan, S. G., Argast, D., Norris, J. E., & Beers, T. C. 2005, *A&A*, 430, 507
- Barklem, P. S., Christlieb, N., Beers, T. C., et al. 2005, *A&A*, 439, 129
- Beers, T. C., Rossi, S., Norris, J. E., Ryan, S. G., & Shefler, T. 1999, *AJ*, 117, 981
- Boesgaard, A. M., Jensen, E. E. C., & Deliyannis, C. P. 2009, *AJ*, 137, 4949
- Bromm, V., Coppi, P. S., & Larson, R. B. 1999, *ApJ*, 527, L5
- Bromm, V., Coppi, P. S., & Larson, R. B. 2002, *ApJ*, 564, 23
- Bromm, V., Yoshida, N., & Hernquist, L. 2003, *ApJ*, 596, L135
- Bromm, V., Yoshida, N., Hernquist, L., & McKee, C. F. 2009, *Nature*, 459, 49
- Cayrel, R., Depagne, E., Spite, M., et al. 2004, *A&A*, 416, 1117
- Cenarro, A. J., Cardiel, N., Gorgas, J., et al. 2001a, *MNRAS*, 326, 959
- Cenarro, A. J., Gorgas, J., Cardiel, N., et al. 2001b, *MNRAS*, 326, 981
- Christlieb, N., Bessell, M. S., Beers, T. C., et al. 2002, *Nature*, 419, 904
- Clark, P. C., Glover, S. C. O., Klessen, R. S., & Bromm, V. 2011a, *ApJ*, 727, 110
- Clark, P. C., Glover, S. C. O., Smith, R. J., et al. 2011b, *Science*, 331, 1040
- Cohen, J. G., Christlieb, N., McWilliam, A., et al. 2004, *ApJ*, 612, 1107
- Dias, W. S., Alessi, B. S., Moitinho, A., & Lépine, J. R. D. 2002, *A&A*, 389, 871
- Ferrara, A., Pettini, M., & Shchekinov, Y. 2000, *MNRAS*, 319, 539
- Frebel, A., Aoki, W., Christlieb, N., et al. 2005, *Nature*, 434, 871
- Fryer, C. L., Woosley, S. E., & Heger, A. 2001, *ApJ*, 550, 372
- Gal-Yam, A., Mazzali, P., Ofek, E. O., et al. 2009, *Nature*, 462, 624
- Gnedin, N. Y. & Ostriker, J. P. 1997, *ApJ*, 486, 581
- Harris, W. E. 1996, *AJ*, 112, 1487
- Heger, A. & Woosley, S. E. 2002, *ApJ*, 567, 532
- Hosokawa, T., Omukai, K., Yoshida, N., & Yorke, H. W. 2011, *Science*, 334, 1250
- Karlsson, T., Bromm, V., & Bland-Hawthorn, J. 2011, *ArXiv e-prints*
- Karlsson, T., Johnson, J. L., & Bromm, V. 2008, *ApJ*, 679, 6
- Lee, Y. S., Beers, T. C., Sivarani, T., et al. 2008a, *AJ*, 136, 2022
- Lee, Y. S., Beers, T. C., Sivarani, T., et al. 2008b, *AJ*, 136, 2050
- Lingenfelter, R. E., Higdon, J. C., Kratz, K., & Pfeiffer, B. 2003, *ApJ*, 591, 228
- Madau, P., Ferrara, A., & Rees, M. J. 2001, *ApJ*, 555, 92
- Moore, C. E., Minnaert, M. G., & Houtgast, J. 1966, *National Bureau of Standards Monograph* 61, 61
- Mori, M., Ferrara, A., & Madau, P. 2002, *ApJ*, 571, 40
- Moultaka, J., Ilovaisky, S. A., Prugniel, P., & Soubiran, C. 2004, *PASP*, 116, 693
- Nakamura, F. & Umemura, M. 2002, *ApJ*, 569, 549
- Ostriker, J. P. & Gnedin, N. Y. 1996, *ApJ*, 472, L63+
- Prugniel, P. & Soubiran, C. 2001, *A&A*, 369, 1048
- Re Fiorentin, P., Bailer-Jones, C. A. L., Lee, Y. S., et al. 2007, *A&A*, 467, 1373
- Smolinski, J. P., Lee, Y. S., Beers, T. C., et al. 2011, *AJ*, 141, 89
- Umeda, H. & Nomoto, K. 2002, *ApJ*, 565, 385
- Wilhelm, R., Beers, T. C., & Gray, R. O. 1999, *AJ*, 117, 2308
- Yoshida, N., Bromm, V., & Hernquist, L. 2004, *ApJ*, 605, 579
- Zhao, G., Zhao, Y.-H., Chu, Y.-Q., Jing, Y.-P., & Deng, L.-C. 2012, *Research in Astronomy and Astrophysics*, 12, 723